Proceedings of The Institute of Acoustics

DESIGN OF A RADIAL ELECTROMAGNETIC BEARING FOR THE VIBRATION CONTROL OF A SUPERCRITICAL SHAFT

V Gondhalekar (1) and R Holmes (2)

(1) Swiss Federal Institute of Technology, Zurich
(2) Department of Mechanical Engineering, University of Southampton

1 INTRODUCTION

The feasibility of using electromagnetic forces to control shaft vibrations has recently been a subject of attention from a number of researchers and successful applications of bearings and dampers in rotating assemblies have been reported [1,2,3]. A flexible transmission shaft needs some form of control to maintain its vibration amplitudes within reasonable limits when passing through its critical speeds. Squeeze-film bearings have been shown to be capable of reducing vibration amplitudes but these can normally only react to the rotor displacement at the bearing locations. A controlled electromagnet (CEM) located at a point along the length of a transmission shaft has also been shown to be effective in reducing vibration amplitudes [2]. The CEM offers the possibility of applying a force which is a function of displacement and/or velocity at the CEM location or at a location remote from it. This allows the implementation of a control strategy which responds to one signal or to the weighted average of more than one signal measurement remote from the CEM location.

The work reported to date on the vibration control of flexible transmission shafts has mainly been concerned with reducing vibration amplitudes. No adaptive control approach has been reported which attempts to manipulate the shaft dynamics to suit the operating conditions. With the availability of fast microprocessors and the inherent control flexibility of the CEM it is feasible to formulate and implement a control strategy which caters for changes in the characteristics of the transmission shaft such as those occurring due to shape distortion and variations in mass unbalance.

Some magnetic bearing configuration proposed by past workers are shown in Fig. 1. The static member of that shown in Fig. 1a is the simplest to construct but, in an attempt to combat eddy current effects, the rotating sleeve must be made from rectangular laminations. Any lamination completing the flux path only does so for a sort time increment and other laminations sequentially perform this function as the shaft rotates. A relatively long axial length is needed to provide a given magnetic force. The radial flux configuration of Fig. 1b makes lamination of both the static and rotating members easy, the latter now being constructed from flat discs. A disadvantage, however, is inefficient radial space utilization. Also the long narrow limbs lead to high magnetic saturation, that is high flux concentration, at the magnet bases.
Magnetic bearings are best designed to operate in an attraction rather than a repulsion mode, but in either case the basic inverse square law relationship between magnetic force and gap has to be overcome since this can lead to instability. Schweitzer [1] describes a design similar to that of Fig. 1b in which stability is achieved, together with the linearity of the force-current characteristic by a differential circuit, in addition to a circuit ensuring premagnetization with a constant current. Thus operation takes place about a

non-zero steady state condition. Easier analysis and controller design are assured by the improvement in linearity but bulky magnets are necessary to dissipate the consequent heat produced by the premagnetization current.

A logical next step is to integrate all four magnets in to a single structure as shown in Fig. 1c. However, there is here a high degree of interaction between the four poles, and consequently the magnet performance has to be improved by special techniques requiring bi-directional drive amplifiers to alter the direction of the flux as required [2]. This disadvantage can be overcome by using the four active/four passive pole congiuration of Fig. 1d [3], in which four uni-directional amplifiers can be used.

Fig. 1e shows a three pole active/three pole passive configuration as used in the present work, as it gives a better space utilization than does that of Fig. 1d, as well as reducing magnet interaction. However, since the magnets do not lie on mutually perpendicular axes, x-y, cross-coupling is introduced between these axes. This is counteracted by suitable software using a microprocessor interface which in any case is essential for adaptive control purposes. Also it was decided to design for operation about a point of zero magnet excitation as this obviates the need for an extra coil to supply a constant magnetizing current. Thus resistive heating of the magnet coils is reduced and also their weight and size. The whole device is required to exert dynamic rather than static force components and hence there is no need from that point of view for non-zero quiescent operating point. One of the main objectives of the present work is to design software to condition the control signals so as to make the magnets appear linear (and uncoupled) in spite of using this zero-excitation point.

The use of digital control requires the specification of the type of system best fitted to the particular application and with it the programming language -high- or low-level. High-level languages require that the computer stores either a compiler or an interpreter program. This presents two difficulties: the computer must have a fairly large storage capacity to store a compiler program or each time the high-level language instruction is executed it must be translated by an interpreter program. This is often too time consuming for real-time control. A low-level language obviates both of these disadvantages since each instruction has a one-to-one relationship with its equivalent machine code instrucation. The result is that the program is executed at very high speed. For this reason and due to economy of memory space, low-level languages are widely used for dedicated microprocessor based systems.
The rotor system controlled by the electromagnets is shown in Fig. 2, and the final electromagnet configuration in Fig. 3. The overall system including the microprocessor and associated peripherals is shown in Fig. 4. The electromagnets, their drive electronics and some results obtained from the rig to date are presented.

2 THE ELECTROMAGNETS AND THEIR DRIVE ELECTRONICS

A block diagram of the electromagnet system designed for the present work is shown in Fig. 5. Each power amplifier, A, which drives a magnet coil, C, is of the switching type, employing pulse-width modulation to reduce power losses. It is designed to operate at a maximum a.c. input of 220 V r.m.s. and as a result approximately 300 V d.c. is available to drive each coil, with a current limit of 10 A, but with available capacity up to 15 A.

The electromagnet configuration of Fig. 3 consists of six radial poles - three active and three passive - the latter acting as return flux paths. The electromagnets and the rotor sleeve were constructed from 0.1 mm disc laminations to eliminate eddy currents up to approximately 300 Hz and the three active poles were suitably energized to generate forces along the x and y axes. This particular configuration was chosen because it utilizes the available radial space more efficiently in terms of force than a similar structure consisting of four active poles, and the number of drive amplifiers is reduced from four to three. One disadvantage is the force interaction introduced between the orthogonal axes, but as mentioned above, software is employed to overcome this problem.

An electromagnet exerts a force approximately proportional to the square of the magnet flux present at the pole face. It is also unstable in an open loop mode since, as the deflection increases towards a magnet, so does the attractive force from that magnet. The system can, however, be made stable by feeding back a signal v_H produced by a Hall probe, which is proportional to the flux at the pole face (Fig. 5). For any given coil and its series resistance, R, the supply voltage, V, is given by:

$$V = L(di/dt) + iR \qquad (1)$$

where L is the inductance of the coil and i the current passing through it. Thus:

$$i/V = (1/R)\ /(\mathcal{L}L/R + 1) \qquad (2)$$

where $\mathcal{L}$ is the Laplace operator.
If we consider, say, magnet No.2, then from Fig. 5:

$$v_{i2} = S_2 - v_{H2} \qquad (3)$$

in which S_2 is the signal voltage from the digital-analogue converter on channel 2 and v_{i2} is the input voltage to the corresponding amplifier. Now the voltage, v_{H2}, generated by the Hall probe is proportional to the flux, ϕ, at the probe face. Also, this flux is proportional to the current, i_2, in the magnet coil and inversely proportional to the gap, z_2, between the magnet face and the shaft. Thus:

$$v_{i2} = S_2 - K_2\phi_2$$

$$v_{i2} = S_2 - K_2K(i_2/z_2)$$

$$v_{i2} = S_2 - K_2K(1/z_2)(V_2/R)(\mathcal{L}L/R+1)^{-1}$$

in which the voltage V_2, supplied to coil $C_2 = av_{12}$, where a is the amplifier gain.

Hence

$$v_{12} = S_2 \Big/ \left[1 + \frac{KK_2 a/R}{z_2(\mathcal{L}L/R+1)} \right]$$

whence

$$\phi_2 = S_2 \Big/ \left[K_2 + \frac{(\mathcal{L}L/R+1)z_2}{aK/R} \right]$$

Hence, if a is large enough, $\phi \propto S_2/K_2$ and is independent of the gap, z_2.

Since the electromagnets can only operate effectively in an attraction mode, with no repulsion, then in order to overcome this undirectional forcing feature in creating restoring forces to counteract displacements Y and X, the excitation signals S_1, S_2 and S_3 to the three drive amplifiers, A, (Fig. 5) would be constituted as follows:

$$\left.\begin{aligned} S_1 &= [Y]_{T/2}^{T} - 0.5[X]_{0}^{T/4} + 0.5[X]_{T/4}^{3T/4} - 0.5[X]_{3T/4}^{T} \\ S_2 &= -[Y]_{0}^{T/2} - [X]_{0}^{T/4} - [X]_{3T/4}^{T} \\ S_3 &= -[Y]_{0}^{T/2} + [X]_{T/4}^{3T/4} \end{aligned}\right\} \quad (4)$$

where T is the periodic time.

These can be understood be referring to Fig. 6a. The top two graphs (a) and (b are the Y and X displacements. Graphs (c) and (d) show, respectively, the terms in Y and X contained in signal S_1. Graphs (e) and (f) show, respectively, the terms in Y and X contained in S_2 and graphs (g) and (h) the terms in Y and X contained in signal S_3.

It will be noted that all three signals contain both X and Y components. This is because magnets No. 2 and No. 3 have to exert forces to counter X and Y displacements, but in the process introduce unwanted X-dependent forces in the Y direction. These are neutralized by additional X-component forces generated in magnet No. 1 by signal S_1. Assuming that a linear relationship exists between the signals and the attraction forces produced by the magnets, then:

$$\uparrow F_y = \alpha[-S_1 + (S_2 + S_3)\cos 60^\circ]$$

$$\rightarrow F_x = (2\alpha/\sqrt{3})[(S_2 - S_3)\cos 30]$$

where α is a constant dependent on the amplifier gains. Fig. 6j shows the way in which F_y is constituted from the terms in Y and it is seen that F_y is a restoring force, that is, it is in opposition to the displacement, Y, of Fig. 6a. Fig. 6k shows that no unwanted force is produced in the X-direction as a result of the terms in Y. Finally, Fig. 6l shows that no unwanted force is

produced in the Y-direction as a result of the terms in X, while Fig.6m shows the way F_x is constituted from the terms in X. It will be seen that F_x is also a restoring force, that is, it is in opposition to the displacement, X, of Fig. 6b.

In fact, the force produced at each pole face is proportional to the square of the flux at that face and hence to the square of the current supplied to each magnet coil. Thus, if there is a linear relation between any signal, S, and its coil current then each magnet force will be proportional to S^2 and not to S as assumed above. However, this can be partially accommodated by replacing the multiplier 0.5 in the first of equations (4) by $\sqrt{0.5}$, the other two equations remaining unaltered. The composite signals, S, thus appear as shown in Fig. 6n. This is followed by writing F_y and F_x as:

$$\uparrow F_y = \alpha \{-(S_1)^2 + [(S_2)^2 + (S_3)^2] \cos 60^\circ\}$$

$$\vec{F}_x = (2\alpha/\sqrt{3}) [(S_2)^2 - (S_3)^2] \cos 30^\circ)$$

As a result, the forms of the forces produced in the x, y directions are shown in Fig. 6p. When combined to produce a polar diagram a significant third harmonic is revealed (Fig. 6q).

Linearization of each magnet device can, however, be achieved by using the square root of the control signal input, S, to each magnet amplifier. This input signal then produces a proportional flux, the appropriate square of which is proportional to the force exerted on the rotor. The control signal S, versus force output thus follows and approximately linear relationship and allows the signal and hence force contributions of the three magnets to be added linearly.

The square root of a number can be found using software by computing a finite number of terms of a series expansion, but this can be time consuming in a real-time application. A piecewise linear approximation to the function $y = K\sqrt{S}$ was therefore used, where S is the control signal, and K is a constant. The above function is divided into thirty-two segments of progressively greater length, since a square root function varies rapidly around zero, and the software computes the square in 96 µs on a Z8002 CPU. The square root procedure, when applied to the control signals of all three magnets results in the polar force diagram shown in Fig. 6r, indicating considerable improvement over that shown in Fig. 6q. The software can be adapted, if required, to compensate for the saturation of the magnet core material.

As well as being influenced by the square law non-linearity, the magnet forces are also subject to current rate saturation in the drive amplifiers. This occurs if more than the maximum drive voltage of the amplifier is demanded. For the inductive loads presented by the magnet coils the current rate, dI/dt, demanded is equal to the quotient, drive voltage divided by inductance, V/L. Now for a current $\hat{I} = I \sin \omega t$:

$$(dI/dt)_{max} = \hat{I}\omega = \hat{V}/L$$

or

$$\hat{I} = \hat{V}/\omega L$$

Thus the output current waveform could become distorted if more than the maximum drive voltage is demanded, resulting in a drop in current gain with increasing frequency and/or input signal amplitude. This is aggravated somewhat by the square root procedure, which demands a higher current rate. In principle, it is possible to condition the amplifier control signals to compensate partially for this rate saturation but this may have a deleterious effect on the stability margins of the device. Fortunately, in practice, the current rates demanded are low enough to be unaffected by any limitation in V, partitularly when the restoring forces provided by the magnets are kept within reasonable limits.

A further potential problem is an additional drop in currrent with increase in frequency due to the L/R time constant of each electromagnet coil and the time constants of the filters in the signal conditioning equipment. However, the bandwidth of the system is around 100 Hz, allowing shaft speeds of up to 6000 r/min, before the performance of the magnet system starts to deteriorate.

Other sources of instability in addition to the time constants of the electromagnet coil and filter, are the delay (zero-order hold) introduced by the micro-computer during manipulation of the sampled signals and the signal clipping due to the finite word length used in the software. Also the loop stability needs to be watched in the context of the switching amplifiers used. These amplifiers, as compared with linear or Class B amplifiers, are more sensitive to the type of load variations experienced in this application, namely the coil inductance variation with rotor displacement.

3 CONTROL STRATEGY

An ideal control strategy would involve the measurement and feedback of all the states (displacement and velocity components of all degrees of freedom) of a rotor system. But even an approximate representation of a rotor system has many degrees of freedom, which might well imply an impracticably large number of measurements. If only two pairs of displacement and velocity components along orthogonal directions are measured, then, assuming an approximate model for the rotor dynamics, an adaptive feedback control can be implemented. The lumped mass construction of the rotor (Fig. 2) makes its mathematical model relatively simple. Assuming negligible internal damping, the rotor vibration can be represented by the following set of equations:

$$y_i = \sum_{j=1}^{j=3} \alpha_{ij}(P_j + m_j \omega^2 y_j) - \alpha_{i4} K_d y_4, \qquad i=1 \text{ to } 4$$

Where α_{ij} are the flexibility influence coefficients (m/N) relating to the mass stations 1, 2 and 3, ω is the rotor speed in rad/s, P_j are the forces due to mass unbalance, y_i are displacement amplitudes at the mass stations and K_d is the stiffness introduced by the CEM at station 4. The negative dynamic stiffness curve at station 4 for this rotor is shown in fig. 7. Dynamic stiffness is the rotor dynamic force at station 4 divided by dynamic displacement, and the frequencies at which the negative dynamic stiffness equals the dynamic stiffness of the support at station 4 are the natural frequencies of the complete system. Thus the intersections with a horizontal line K_d parallel to the ω-axis give the natural frequencies ω_n (that is critical speeds) of the rotor system.

VIBRATION CONTROL OF A SUPERCRITICAL SHAFT

The frequency response of the displacement at station 1 to mass unbalance force $P_1 = 0.1 \times 10^{-2} \times \omega^2$ is shown in Fig.8 both for $K_d = 0$ and for $K_d = 0.5 \times 10^6$ and, as in Fig. 7, indicates the shift in natural frequencies due to the change in stiffness. A speed-dependent controller can ensure that the natural frequencies of the rotor system are sufficiently removed from the mass unbalance disturbance frequency (that is the rotational speed) by automatically adjusting the stiffness, K_d.

It is also possible to introduce both stiffness and damping at station 4. If the force F_4 is made a linear function of both y_4 and $\dot{y}_4$ i.e.

$$F_4 = - K_2(K_d\, y_4 + K_v\, \dot{y}_4)$$

then the resulting root locus of the rotor system with increasing values of is shown in Fig. 9 for two different values of K_d/K_v. The intersection of a particular root locus curve and the critical damping line suggests an ideal operating point for that particular natural frequency and illustrates a more comprehensive approach towards implementing an adaptive controller. It may be noted from Fig. 9 that the third natural frequency is influenced very little by the feedback coefficients. This is because station 4 is located very near to one of the nodal points of the third mode of vibration. If a CEM with displacement and velocity sensors were located at such a nodal point, this particular mode would be both unobservable and uncontrollable.

The continuing research programme will include an investigation of the controllability and observability of the rotor modes at different, not necessarily coincident, locations of the CEM and the sensor units. This study will then be extended to formulate a state observer which would enable an estimation to be made of the rotor states from a minimum number of measurements. These state estimates will then be used to implement the second of the above mentioned control stategies, namely, an optimal controller using the model follower technique. Knowing the influence coefficient matrix of the rotor and the vibration amplitudes at a rotational speed sufficiently removed from a critical speed, it should be possible to estimate a representative mass unbalance on the rotor. As the mass unbalance is the source of the disturbance inputs to the shaft, an optimal control algorithm could be formulated such as to counteract the disturbance in a suitable manner. With the CEM unit as an actuator and the numerical capability of the microprocessor it should be possible to implement a system identification algorithm which would determine variations in rotor characteristics, such as the mass unbalance, and make suitable alterations to the control algorithm. The algorithm could be made adaptive in the sense that it could follow a stategy whose attributes are suitable for traversing the particular speed at which the rotor is operating. Fig. 10 shows some typical response curves taken from the rotating assembly of Fig. 2, sample values of stiffness and damping provided by the controlled electromagnets being indicated. These serve to indicate how the critical speeds can be altered and the peak responses brought down to acceptable levels.

4 CONCLUSIONS

The results of this research indicate that efficient and compact electromagnets have been designed to control the vibrations of a supercritical rotating assembly in an effective manner. By the use of a microprocessor, software has been designed to overcome any problems of cross-coupling between othogonal axes and of inherent non-linear force-deflection characteristics in the magnets. By the same microprocessor a considerable degree of control can also be achieved, as indicated in Fig. 10.

The research programme will be continued with a view to formulating and implementing suitable control schemes and it is expected that the information and experience so gained will be applicable to a variety of transmission shaft configurations.

REFERENCES

[1] SCHWEITZER, G. and ULBRICH, H. Magnetic bearings - a novel type of suspension. Vibrations in Machinery, Instn Mech. Engrs conference, 1980, Paper C273/80, pp 151-156

[2] NIKOLAJSEN, J N, HOLMES, R and GONDHALEKAR, V. Investigation of an electromagnetic damper for vibration control of a transmission shaft. Proc. Instn Mech. Engrs, 1979, 193, 331-336.

[3] HABERMANN, H. Le Palier magnetique actif 'ACTIDYNE'. Problems in bearings and lubrication, Ottawa, Canada May 1982, AGARD Conference Proceedings No 323.

ACKNOWLEDGEMENTS

This paper has described an ongoing programme of research conducted at the University of Sussex and at the University of Southampton. Thanks are due to these establishments for providing research facilities and to the Science and Engineering Research Council for financial support. The authors are also grateful to Professor B V Jayawant for valuable discussions during the course of the research.

VIBRATION CONTROL OF A SUPERCRITICAL SHAFT

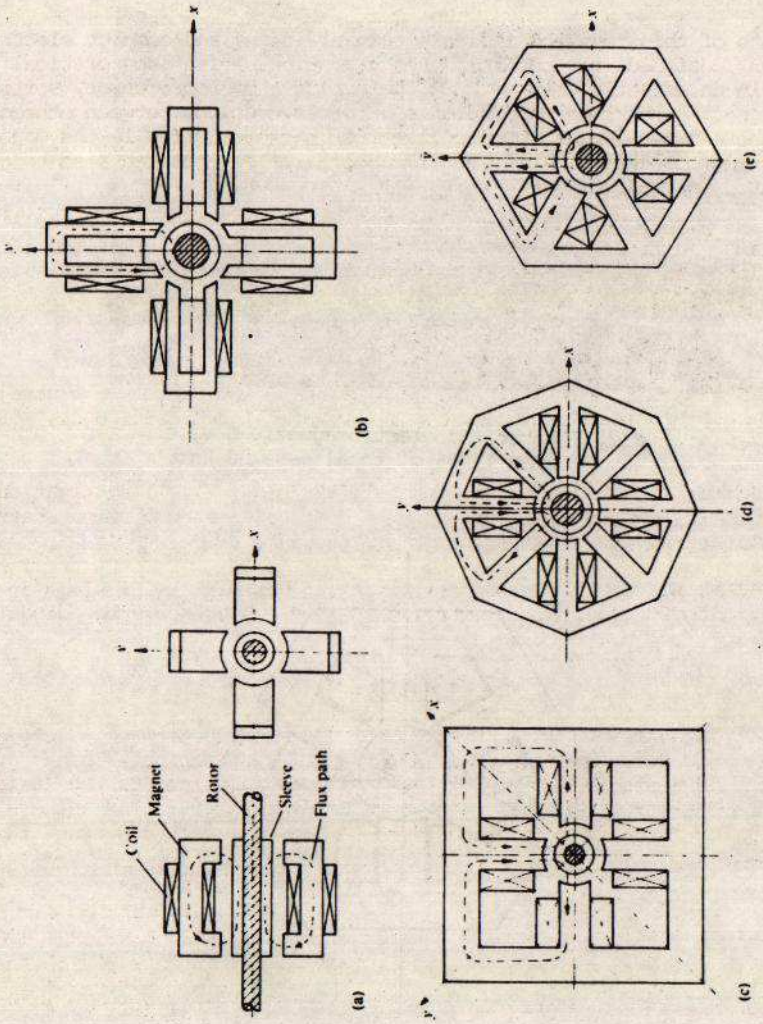

Fig. 1 Viable magnetic bearing configurations

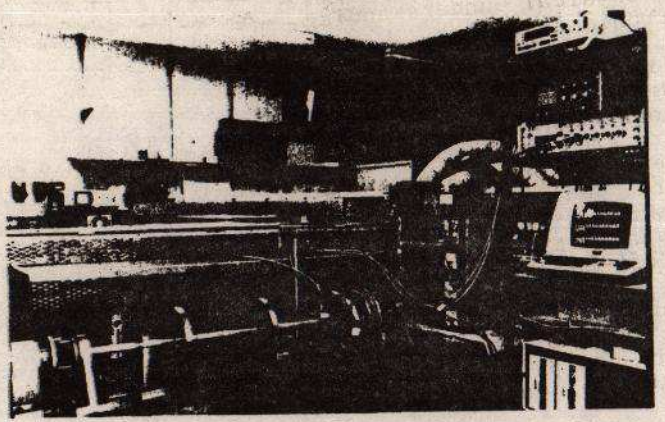

Fig. 2 Rotor and electromagnetic device:
span 1.256 m, total mass 30 kg

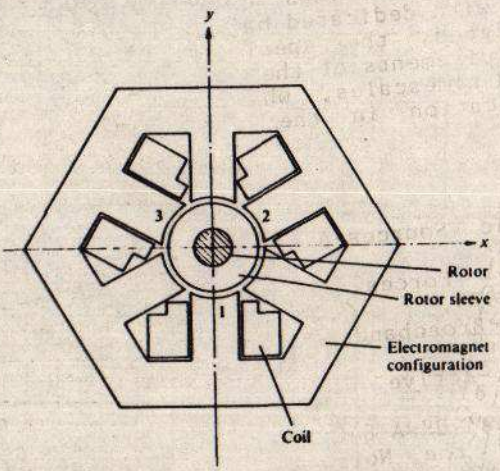

Fig. 3 Active pole electromagnetic configuration:
radial air gap 2 mm, radial stiffness
1-10 x 10^5 N/m
peak power requirement 200 W

VIBRATION CONTROL OF A SUPERCRITICAL SHAFT

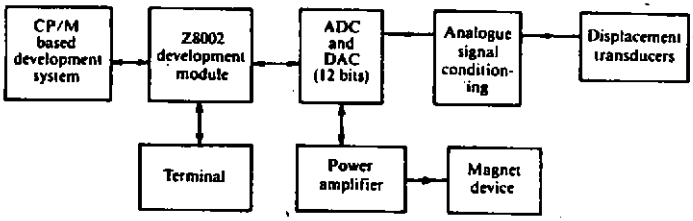

Fig. 4 The computer and electromagnetic system

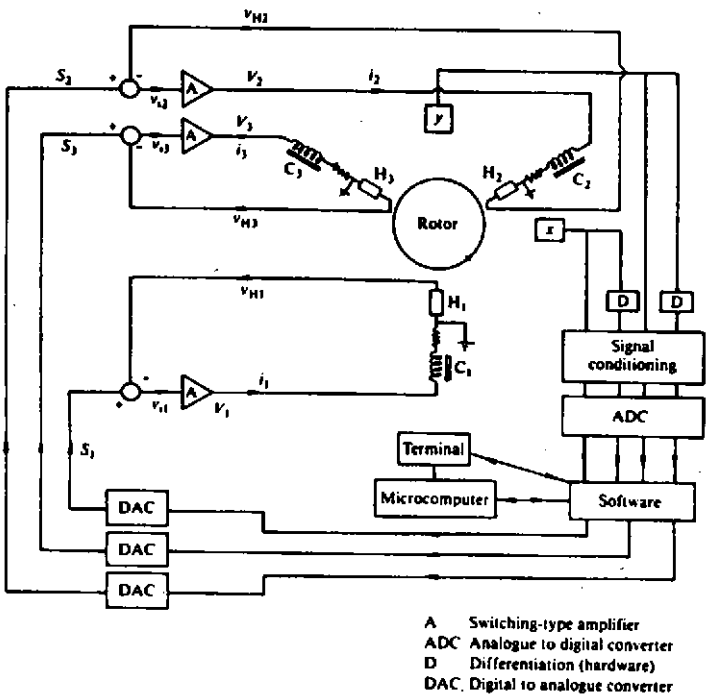

Fig. 5 Electromagnetic system

VIBRATION CONTROL OF A SUPERCRITICAL SHAFT

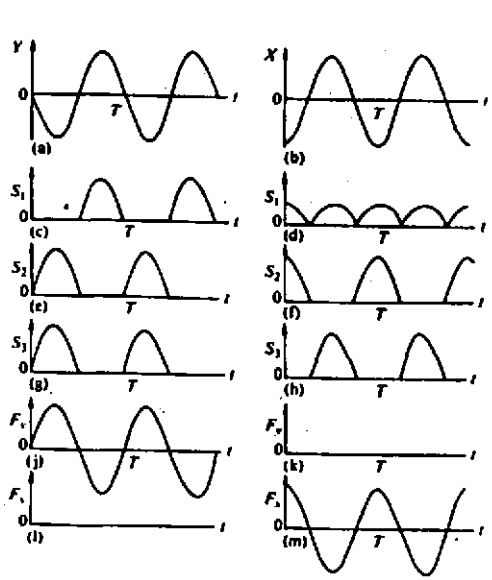

Fig. 6a-m Content of signals

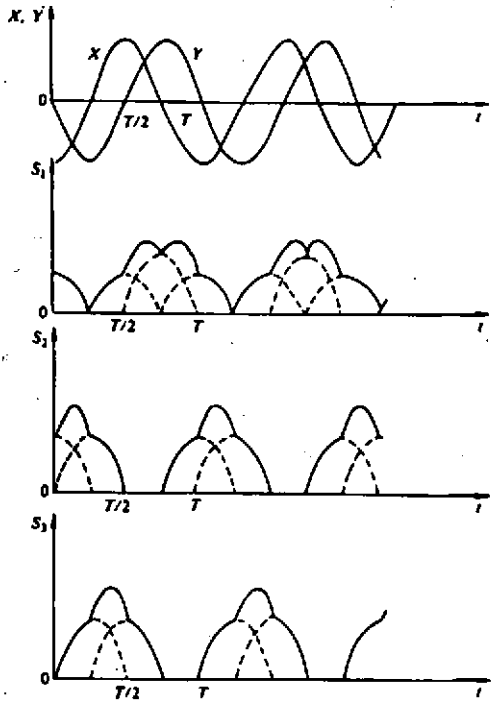

Fig. 6n Excitation signals

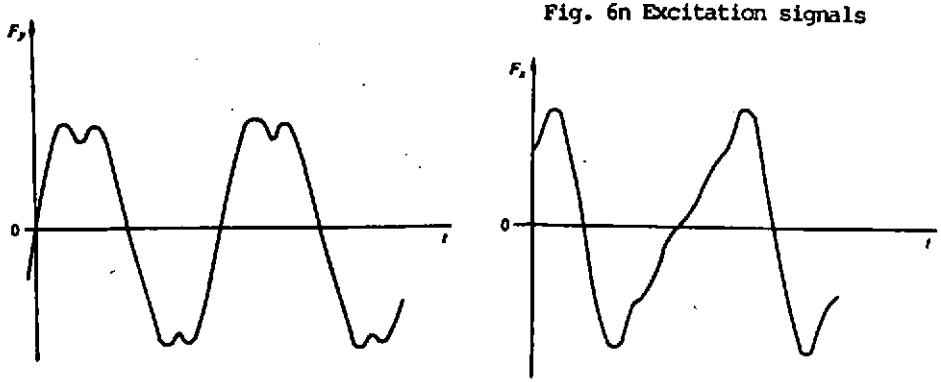

Fig. 6p Forces in orthogonal directions

VIBRATION CONTROL OF A SUPERCRITICAL SHAFT

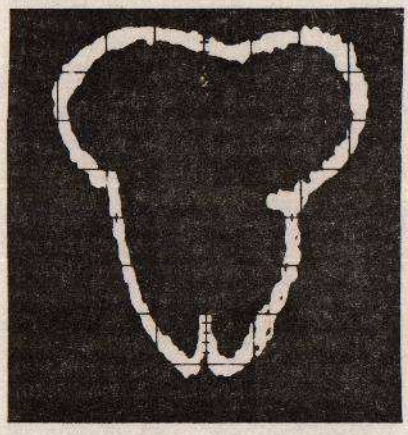

Fig. 6q Polar force diagram

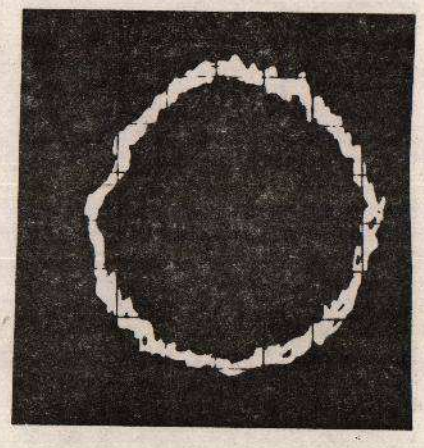

Fig. 6r Improved polar force diagram

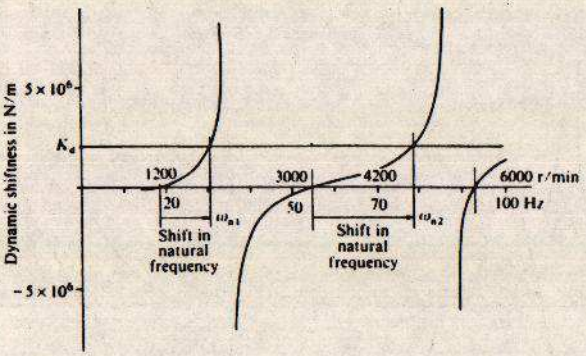

Fig. 7 Negative dynamic stiffness curve and shifts in natural frequency due to K_d

VIBRATION CONTROL OF A SUPERCRITICAL SHAFT

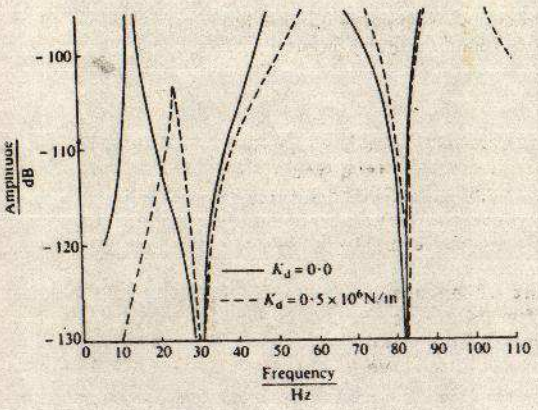

Fig. 8

Frequency response to mass unbalance

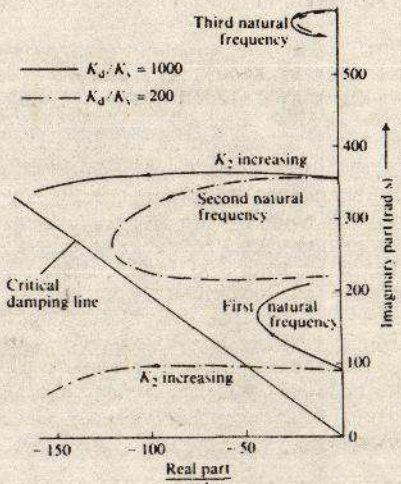

Fig. 9 Root locus of flexible shaft with CEM at station 4

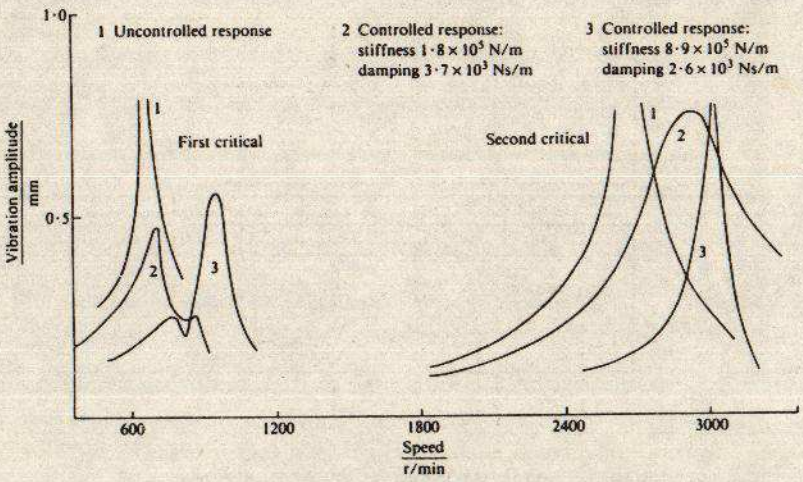

Fig.10 Typical response curves

Proceedings of The Institute of Acoustics

COMPUTER SIMULATION IN ACTIVE NOISE CONTROL

P. Sjösten (1), P. Eriksson (2) and I. Claesson (2)

(1) Dept of Acoustics, Chalmers Univ of Techn, Gothenburg, Sweden
(2) Dept of Telecom Theory, Lunds Univ of Techn, Lund, Sweden

In the recent developement of active noise control systems, adaptive digital filters have become widely used. The reason for this is quite natural, since the properties of acoustic systems tend to vary (depending on temperature, etc) with time and since adaptive filters have the ability to change their properties continuously according to some minimization criteria.

Figure 1 shows the simplest possible layout of an active noise control system. $H_{x\varepsilon}$ is the acoustic frequency response function from the source signal, x to the residual output signal, ε and $\hat{H}_{x\varepsilon}$ is the filter response. The residual output from the noise canceller is used by the adaptive filter to optimise its response.

The residual error can be minimized according to different criteria. One is the least mean square (LMS) criterion, in which the mean output power is minimized. A number of algorithms based on this criteria have been published, as well as papers concerning their convergence properties, e.g. [1] [2].

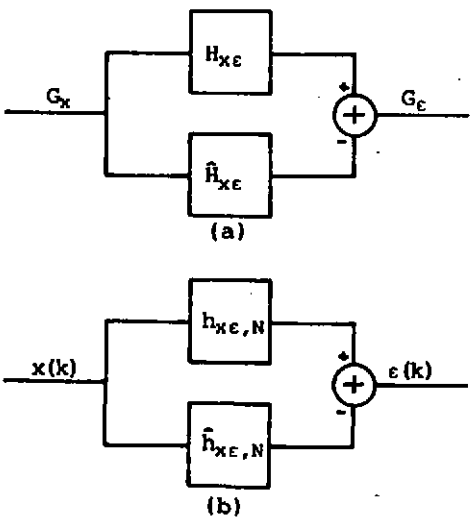

Figure 1. Simple model of an ANC system.
a) frequency domain, frequency response functions
b) time domain, impulse response functions.

COMPUTER SIMULATION

No matter what criterion is used, the algorithm is most often based on the presupposition that the digital filter is a transversal filter since this kind of filter is well suited for adaptive implementation.

Equation 1 shows the general form of the frequency response of a transversal filter.

$$H(f) = \sum_{n=0}^{N-1} c_n H_n(f) \qquad (1)$$

where for a common FIR filter

$$H_n(f) = e^{j2\pi fn} \qquad (2)$$

and c_n is real.

Many acoustic systems show resonant behaviour in the frequency response function, and for these systems, it may be advantageous to choose a filter function with resonant character, instead of the one specified in eq 2. One may, for example, choose a $H_n(f)$ according to equation 3,

$$H_n(f) = H_o(f-n\Delta f), \qquad n_1 \leq n \leq n_2, \quad 0 \leq n_1 \leq n_2 \leq N-1 \qquad (3)$$

$$H_o = \begin{cases} 1 - |f/\Delta f|, & |f| \leq \Delta f \\ 0, & \text{elsewhere} \end{cases}$$

One method of evaluating the results for different filter functions, is by means of computer simulation. The corresponding time-domain functions to those specified in figure 1a, are shown in figure 1b. The impulse response $h_{Xe,N}$ is calculated as the inverse transform of the frequency response function, $H_{Xe}(f)$. The later function can easily be measured, e.g. with an FFT analyser.

The two functions are fed with noise from the same source, and the spectrum of the noise, G_X, is filtered to have the same spectral density as the primary noise source.

By studying figure 2, we can directly compare the results from two computer simulations, using the filter functions in eqs 2 and 3 respectively.

Fig 2a shows the measured transfer function, displayed for that part of the frequency domain where $G_X(f)$ is not zero. Figures 2b and c demonstrates the response of the two adapted filters, both having a filter length, N, of 38.

COMPUTER SIMULATION

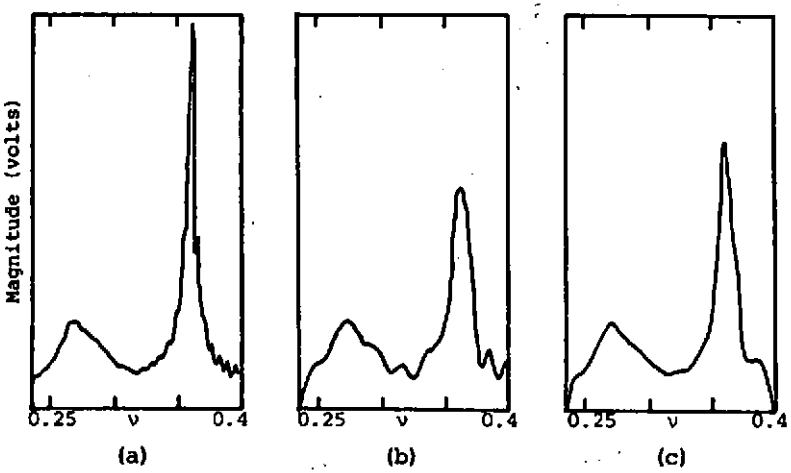

Figure 2. ν is the normalized frequency, f/f_s, f_s is the sampling frequency.
a) measured frequency response
b,c) computed response

From figure 2 we can draw the conclusion that the filter function in eq 3 is a better choice for this particular case, since the adaptive filter response shows a better agreeement to the measured response using this function.

The simple layout in figure 1 may be good for a first approximation, or a first check of different filter functions. A more accurate prediction of the efficiency of the system requires a better model of the complete system. An improved model is shown in figure 3a.

Here, we have incorporated two transfer functions, H_1 and H_2. These include the properties of microphones, loudspeakers, anti-aliasing filters, amplifiers, etc, and specifically for H_2, the acoustic transfer function between secondary source and ϵ.

By rearraging the blocks according to figure 3b, we now obtain the optimal solution for $\hat{H}_{xs}$ as

$$\hat{H}_{xs}(f) = H_{x\epsilon} \; / \; H_1 H_2 \qquad (4)$$

Using this model, three frequency response functions are measured, $H_{x\epsilon}$, H_1 and H_2. $\hat{H}_{xs}$ is then formed according to equation 4 and its inverse is calulated, as before.

COMPUTER SIMULATION

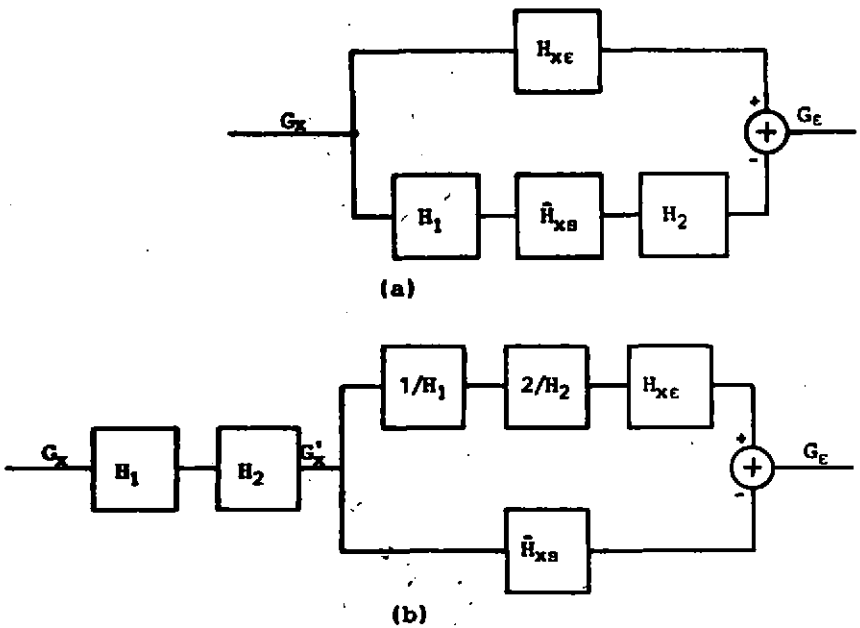

Figure 3. Improved model of the ANC system
a) straight forward form
b) rearranged form.

We have by this manipulation reduced our improved model to the simple model in figure 1, but now with a different input signal and another optimal frequency response.

A computer simulation, using this compounded frequency response function, may point at the necessity to further "improve" the filter function to obtain an optimal fit between the "true" frequency response function and the response of the adaptive filter.

REFERENCES:

[1] "Adaptive signal processing", B Widrow, S D Stearns, Prentice Hall, 1985

[2] "Adaptive Filterting, Prediction and Control", G C Goodwin, K S Sin, Prentice Hall, 1984